CHEMISTRY
A EUROPEAN JOURNAL

DOI: 10.1002/chem.200902231

Regiocontrolled Synthesis of Ethene-Bridged *para*-Phenylene Oligomers Based on Pt^{II}- and Ru^{II}-Catalyzed Aromatization

Tse-An Chen,[a] Te-Ju Lee,[b] Ming-Yuan Lin,[a] Shariar M. A. Sohel,[a] Eric Wei-Guang Diau,[b] Shie-Fu Lush,[c] and Rai-Shung Liu*[a]

Abstract: We report the regiocontrolled syntheses of ethene-bridged *para*-phenylene oligomers in three distinct classes by using Pt^{II}- and Ru^{II}-catalyzed aromatization. This synthetic approach has been developed based on twofold aromatization of the 1-aryl-2-alkynylbenzene functionality, which proceeds by distinct regioselectivity for platinum and ruthenium catalysts. Variable-temperature NMR spectra provide evidence that large arrays of these oligomers are prone to twist from planarity. The UV/Vis and photoluminescence (PL) spectra as well as the band gaps of these regularly growing arrays show a pattern of extensive π conjugation with increasing array sizes, except for in one instance.

Keywords: catalysis · platinum · polyaromatic oligomers · regiocontrol · ruthenium

Introduction

Benzenoid polycyclic aromatic hydrocarbons (BPAHs) have found widespread applications in various photoelectronic devices.[1] Progress in the synthesis of discotic molecules[1,2] of BPAHs has been more successful than ribbon-type fused benzenes that are best represented by heptacene[3] **1**, as depicted in Scheme 1. Despite their outstanding performance in organic thin-film transistors (OTFT), large polyacenes are strictly restricted to heptacene because of their high instability and insolubility.[4]

We sought to prepare new ribbon-type BPAHs[5,6] based on ethene-bridged *para*-phenylene frameworks,[7] which have structures with two central benzene units (A–E) linked by a HC=CH unit as shown in **2** in Scheme 1. Synthesis of such benzene arrays is challenging because possible stereoisomers rapidly grow with the increasing number of benzene units. The important application of such oligomers is demonstrated by the remarkable OTFT performance of picene (**3**),

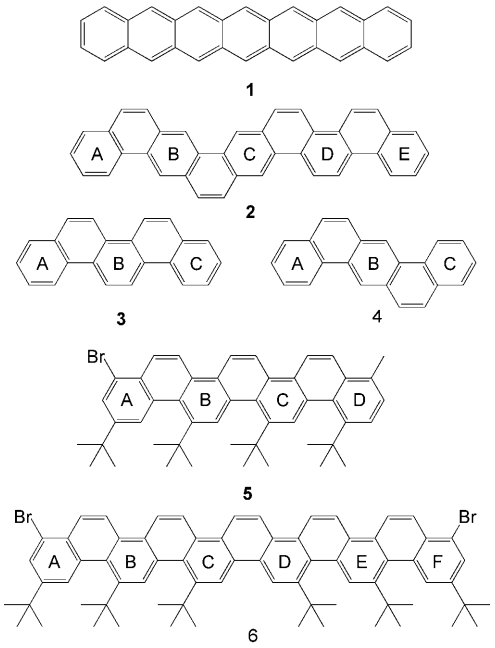

Scheme 1. Polyacenes **1** and ethene-bridged *para*-phenylene oligomers **2**–**6**.

[a] Dipl.-Chem. T.-A. Chen, Dr. M.-Y. Lin, Dr. S. M. A. Sohel, Prof. Dr. R.-S. Liu
Department of Chemistry, National Tsing-Hua University
Hsinchu, 30013, Taiwan (R.O. China)
Fax: (+886) 3-5711082
E-mail: rsliu@mx.nthu.edu.tw

[b] Dr. T.-J. Lee, Prof. Dr. E. W.-G. Diau
Department of Applied Chemistry
National Chiao-Tung University
Hsinchu, 30010, Taiwan (R.O. China)

[c] Prof. Dr. S.-F. Lush
Department of Medical Technology, Yuanpei University
Hsinchu, 30015, Taiwan (R.O. China)

Supporting information for this article is available on the WWW under http://dx.doi.org/10.1002/chem.200902231.

WILEY InterScience DISCOVER SOMETHING GREAT
© 2010 Wiley-VCH Verlag GmbH & Co. KGaA, Weinheim

even in air at room temperature.[7] Before the present work was conducted, the syntheses of such oligomers was only reported for **3**, dibenzo[a,h]anthracene (**4**), highly twisted phenacene (**5**),[7] and [11]phenacene (**6**).[6c–e] Here, we report the first regiocontrolled synthesis of such new polyaromatic oligomers based on platinum- and ruthenium-catalyzed aromatization reactions.

Results and Discussion

Scheme 2 shows our targeted oligomers, represented by **A3**, **A5** and **A7**, with the bridged ethene groups on opposite sides with respect to the central C_2 axis. We also prepared the intermediates **A4** and **A6** to examine their compatibility with this family. Detailed procedures for the synthesis of the starting substrates **A4s**–**A7s** are provided in the Supporting Information. As shown in Scheme 3, these substrates comprise a central benzene tethered by two propynyl groups for twofold aromatization. The tethered methyl groups are crucial to prepare the heavier congeners **A6** and **A7** because they lead to the improved solubility of starting substrates **A6s** and **A7s**. The catalyst $PtCl_2/CO$[8] was selected because it was reported to be the best catalyst for such an aromatization through a π-alkyne intermediate. We found that the platinum catalyst provided excellent regioselectivity and satisfactory efficiency through attack of the more hindered (*peri*) C–H carbon of the naphthalene and other fused aromatic arrays at the propyne groups. The large HOMO orbital coefficients of these C–H carbons control the observed regioselectivity.[9] The structures of these air-stable yellowish products **A3**–**A7** were elucidated by ^{1}H-NOE spectroscopy and MALDI-mass spectra (see the Supporting Information). The ^{1}H NMR signals of species **A7** are concentration dependent, presumably caused by molecular aggregation in solution. The proton signals of **A7** are shifted upfield in highly concentrated solutions, with a $\Delta\delta$ up to 0.2–0.3 ppm in the range of 2.5×10^{-3}–1.0×10^{-2} M.[10]

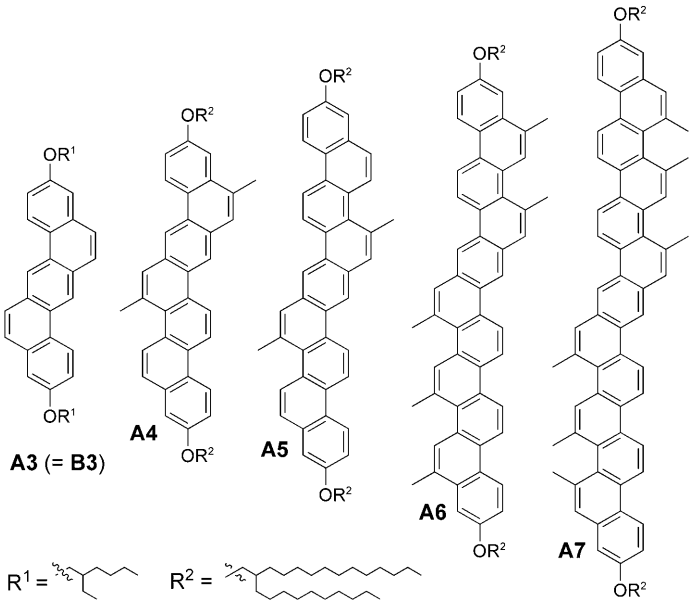

Scheme 2. Targeted ethene-bridged *para*-phenylene oligomers.

Scheme 4 shows the preparation of additional ethene-bridged *para*-phenylenes in new classes, represented by **B3**–**B5** and **C3**–**C5**. The former has two adjacent ethene groups on opposite sides, whereas the latter have the bridged ethylene groups all on the same side. The preparation of **B3**–**B5** was accomplished by the use of $[Ru(CH_3CN)_2(PPh_3)Tp][SbF_6]$ (Tp = tris(1-pyrazolyl)borate) to catalyze the aromatization of substrates **B3s**–**B5s**. This catalyst was selected because it activates the aromatization of 3,5-dien-1-ynes via a ruthenium–vinylidene intermediate.[11,12] We were surprised to find that the aromatization proceeded through an addition of the less-hindered C–H bond of the central aromatic arrays to the adjacent terminal alkynes;[6d] this regioselectivity is completely distinct from platinum chemistry. We assume that the bulky {Ru(PPh$_3$)Tp} fragment alters this aromatization regioselectivity.[10] Syntheses of the oligomers **C3**–**C5** were accomplished through the $PtCl_2$-catalyzed aromatization of substrates **C3s**–**C5s**. The regioselectivity resembles that seen for species **A3**–**A7**. Compounds **B3**–**B5** and **C3**–**C5** were characterized by NMR spectroscopy and

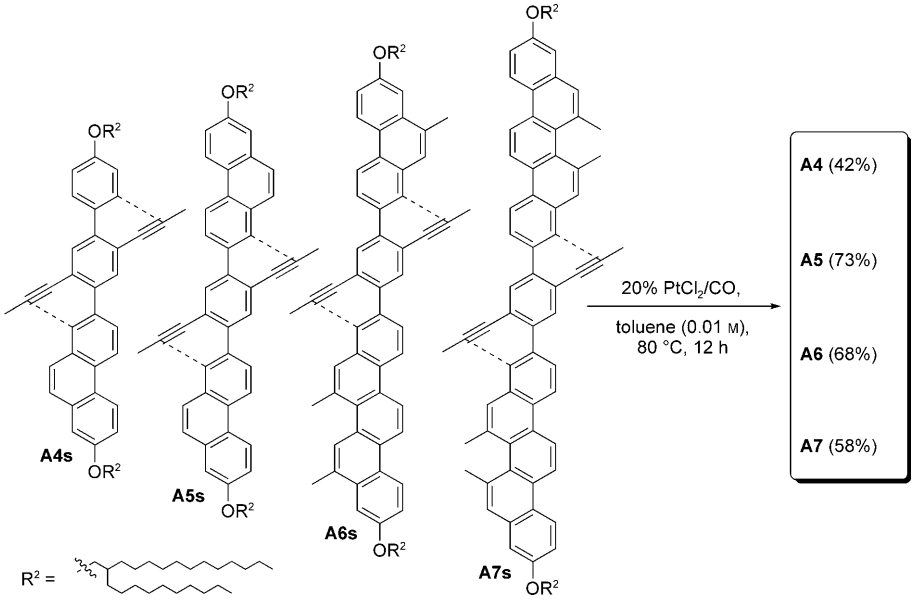

Scheme 3. Platinum-catalyzed regiocontrolled synthesis of series **A**.

 © 2010 Wiley-VCH Verlag GmbH & Co. KGaA, Weinheim

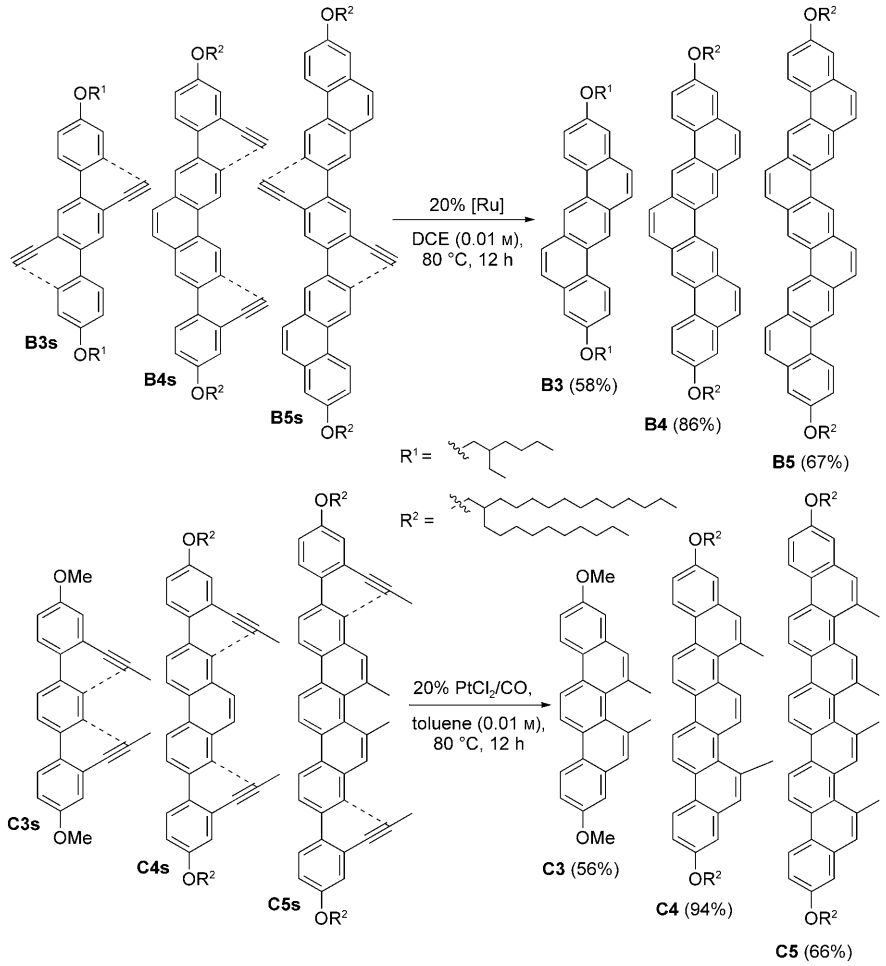

Scheme 4. Regiocontrolled synthesis of oligomers of **B** and **C** series with ruthenium and platinum catalysts.

isomers as shown by its variable-temperature ^{1}H NMR spectra (Figure 1). The activation energy ($\Delta G^{\neq}$) was estimated to be 14.2 kcal mol^{-1}. To understand the size effect on the planarity twist, we prepared a medium ribbon **A5′** that showed ^{1}H NMR signals of two stereoisomers in a 1:1 ratio at 25 °C, with each isomer having a C_2 or S_2 axis as depicted in Scheme 5. As depicted in Figure 2, these NMR peaks became coalesced to signals of one single species as the temperature was gradually brought to 105 °C, due to a rapid α–β exchange. The kinetic parameters of this variable-temperature NMR investigation gave a large vaule of $\Delta G^{\neq} = 19.6$ kcal mol^{-1}.

Figure 3a shows the steady-state UV/Vis absorption spectra of BPAHs **A3**–**A7** and their corresponding photophysical properties are summarized in Table 1. The absorption maxima gradually move to large wavelengths with an increase of the molecule length

MALDI mass spectrometry (see the Supporting Information). For oligomers of the series **B** and **C**, attempts to synthesize their heavier congeners were unsuccessful because of the poor solubility of the starting substrates.

For species **A7**, we observed ^{1}H NMR signals of only one coalesced species at 25 °C although the two adjacent methyl pairs create two axial chiralities. The interconversion of the two stereoisomers, through a twist of planarity,[13] is probably very fast in such a large array. This hypothesis was verified by cooling the NMR temperature to −25 °C, at which the coalesced peaks of **A7** were split into separate signals of the two stereo-

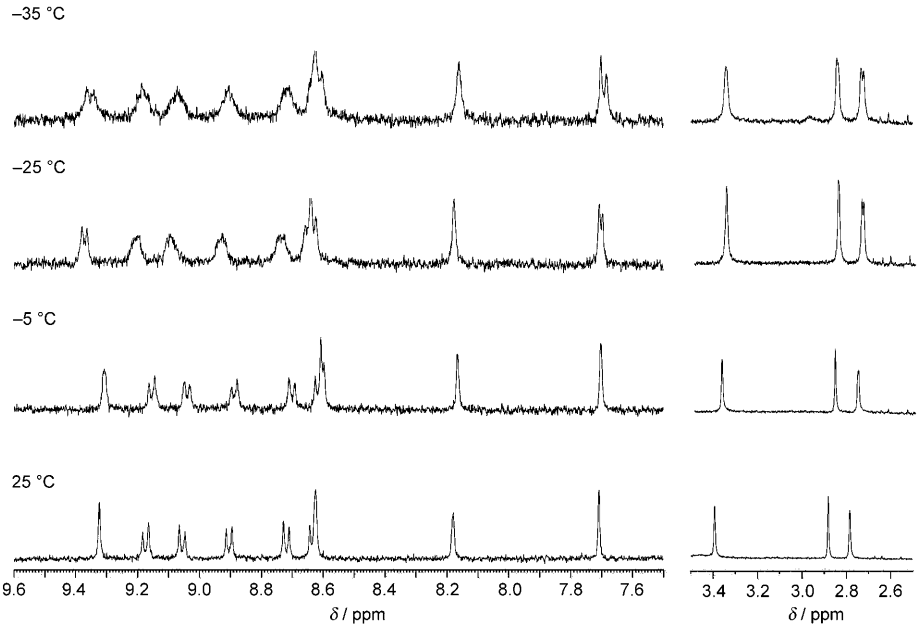

Figure 1. Variable-temperature ^{1}H NMR spectra of compound **A7** in 1:1 CS_2/CD_2Cl_2 (500 MHz) from 25 to −35 °C. The NMR signals in the $\delta = 2.7$–3.5 ppm correspond to six methyl signals.

© 2010 Wiley-VCH Verlag GmbH & Co. KGaA, Weinheim

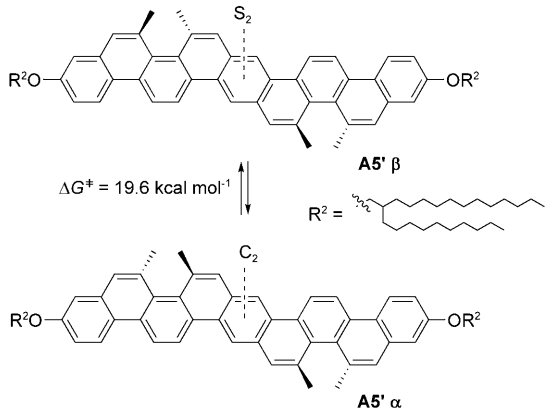

Scheme 5. Planarity twist of oligomer **A5′**.

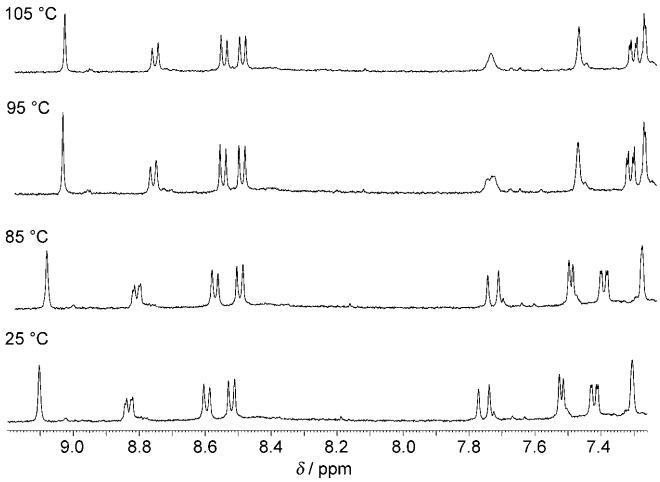

Figure 2. Variable-temperature ^{1}H NMR spectra of compound **A5′** in $CDCl_3$ from 25 to 105 °C.

(*d*) from 1.16 to 2.88 nm from **A3** to **A7**. The large arrays **A6** and **A7** have low extinction coefficients in their UV/Vis absorptions, which presumably arise from molecular aggregation because of their low solubility. Figure 3b shows the un-normalized emission spectra of these *para*-phenylene

Table 1. Photophysical properties of compounds **A3**–**A7**.

	A3	A4	A5	A6	A7
d [nm]	1.16	1.59	2.02	2.45	2.88
λ_{max} (log ε)	308 (5.16)	331 (4.99)	346 (5.14)	353 (4.14)	364 (4.51)
λ_{S_1} (log ε)[a]	402 (3.29)	417 (3.12)	430 (3.45)	436 (3.00)	443 (3.32)
λ_{em} [nm][b]	403	418	430	438	444
ΔE [eV][c]	3.07	2.97	2.88	2.84	2.80
HOMO [eV]	5.57	5.45	5.42	5.36	–
LUMO [eV]	2.50	2.48	2.54	2.52	–
Φ_F[d]	0.21	0.17	0.19	0.38	0.23
τ_s [ns][e]	10.56	15.80	11.29	9.01	8.13
τ_r [ns][f]	51.26	92.94	58.80	23.71	35.34

[a] The absorption peaks of the lowest electronic states (S_1). [b] Emission spectra excited at 375 nm. [c] ΔE = energy gap. [d] Fluorescent quatum yield measured relative to 9,10-diphenylanthracene. [e] Exicted-state lifetime. [f] Radiative rate coefficients.

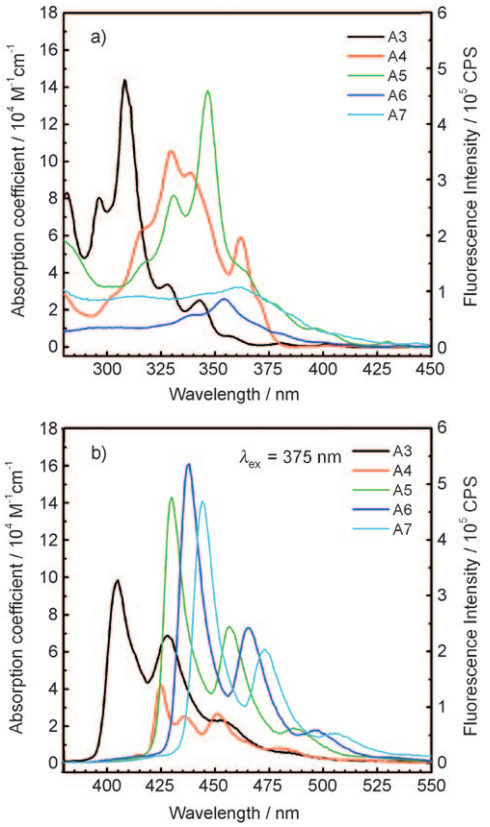

Figure 3. a) UV/Vis absorption spectra of **A3**–**A7** in CH_2Cl_2. b) Unnormalized fluorescence spectra obtained at excitation of 375 nm.

oligomers that comprise successive vibronic structures even for the largest species **A7**, indicating the rigidity of the ribbon structures. Species **A3** shows a maximum at 403 nm, which is consistently shifted to larger wavelengths with increasing array size until a maximum is reached at λ_{em} = 444 nm for **A7**. Compounds **A3**–**A7** are very fluorescent with Φ_F = 0.17–0.38. These quantum yields are well correlated with their radiative rate coefficients expressed by τ_r. The long excited-state lifetimes (8.13–15.8 ns) are characteristic of BPAHs. We estimated the HOMO energy levels of species **A3**–**A6** from their oxidation potentials ($E^{ox}_{1/2}$), and obtained the LUMO energy levels from the measured energy gaps provided by the UV/Vis spectra. The poor solubility of species **A7** meant that its HOMO level could not be determined.

The lowest electronic states (S_1–S_0) of **A3**–**A7** could be recognized from their weak absorption coefficients (log ε = 4.14–5.16). We determined the band gap (ΔE) of each compound from the middle position between the S_1–S_0 absorption and the emission peaks and the results are summarized in Figure 4, which shows a plot of ΔE versus $1/n$ (n = the number of central benzene moieties).[14] A nearly straight line was established for **A3**–**A7**, confirming the compatibility of such a family.

We also examined the photophysical properties of **B3**–**B5** and **C3**–**C5** with their UV/Vis and PL spectra, and key data

 © 2010 Wiley-VCH Verlag GmbH & Co. KGaA, Weinheim

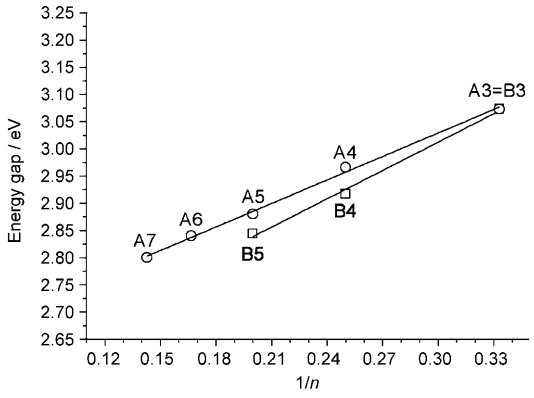

Figure 4. Plot of the energy gaps (eV) versus $1/n$ (n = number of central benzenes) for **A3**–**A7** and **B3**–**B5**.

given in Figures 5 and 6 and Table 2. As we expected, most of these compounds show a pattern of extensive π conjugation with increasing array size except for species **C3**, which has a larger emission wavelength (λ_{em} = 428 nm) than those of **C4** (λ_{em} = 416 nm), **A3** (λ_{em} = 403 nm), and **B3** (λ_{em} = 403 nm), all of which have the same array size. Furthermore, the UV/Vis absorption of **C3** has a very small absorption coefficient ($\log\varepsilon$ = 4.79) although the absorption wavelength (λ_{max} = 302 nm) is smaller than that of **C4** (λ_{max} = 317 nm).

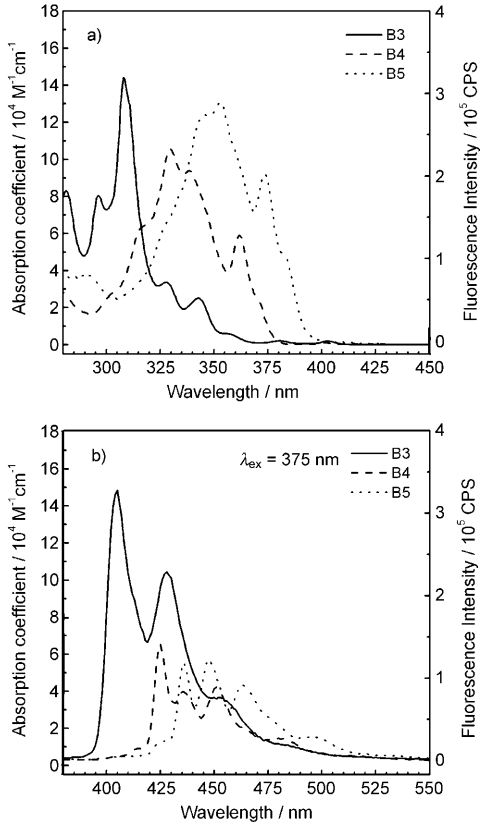

Figure 5. a) UV/Vis absorption and spectra of **B3**–**B5** in CH_2Cl_2. b) Unnormalized fluorescence spectra obtained at excitation of 375 nm.

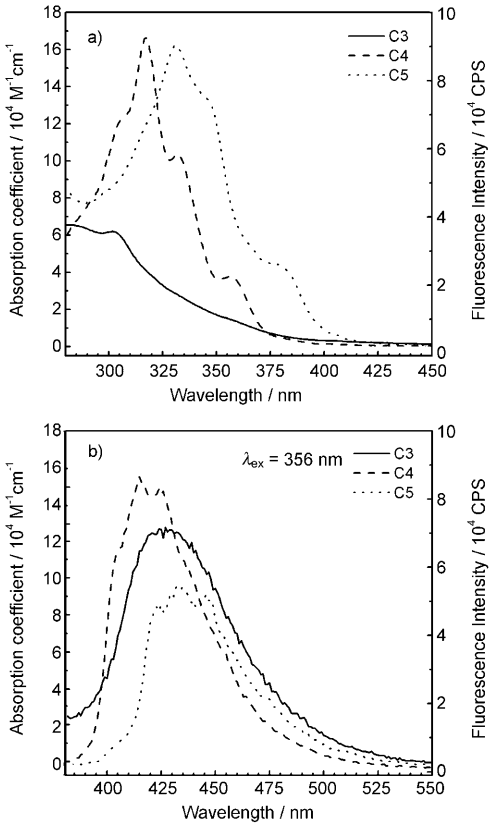

Figure 6. a) UV/Vis absorption and spectra of **C3**–**C5** in CH_2Cl_2. b) Unnormalized fluorescence spectra obtained at excitation of 356 nm.

Table 2. Photophysical properties of compounds **B3**–**B5** and **C3**–**C5**.

	B3	**B4**	**B5**	**C3**	**C4**	**C5**
d [nm]	1.16	1.59	2.02	1.14	1.59	2.01
λ_{max} ($\log\varepsilon$)	308 (5.16)	329 (5.02)	353 (5.11)	302 (4.79)	317 (5.22)	330 (5.20)
λ_{S_1} ($\log\varepsilon$)[a]	402 (3.29)	425 (2.75)	434 (2.63)	–	–	–
λ_{em} [nm][b]	403	425	436	428	416	435
ΔE [eV][c]	3.07	2.92	2.84	–	–	–
HOMO [eV]	5.70	5.47	5.67	5.86	5.76	5.53
LUMO [eV]	2.50	2.55	2.83	–	–	–
Φ_F[d]	0.21	0.11	0.09	0.10	0.086	0.082
τ_s [ns][e]	10.56	31.80	27.95	13.57	17.31	13.04
τ_r [ns][f]	51.26	289.09	310.55	135.16	201.27	159.48

[a] The absorption peaks of the lowest electronic states (S_1). [b] Emission spectra excited at 356 and 375 nm. [c] ΔE = band gap. [d] Fluorescence quantum yield measured relative to 9,10-diphenylanthracene (**B3**–**B5**) and anthracene (**C3**–**C5**). [e] Exicted-state lifetime. [f] Radiative rate coefficients.

Species **C3**–**C5** are particularly notable for their small quantum yields (0.082–0.10), large radiative rate coefficients (τ_r = 135–202 ns), and the loss of their vibronic structures in PL emission. We were not able to obtain accurate energy gaps for species **C3**, **C4**, and **C5** because of their unrecognizable S_1–S_0 band. A plot of band gaps versus $1/n$ (Figure 4), nevertheless, indicated a well-matched convergence of these oligomers of series **B** (**B3**, **B4**, and **B5**). We envisaged that the

 © 2010 Wiley-VCH Verlag GmbH & Co. KGaA, Weinheim

methyl groups of the oligomers of series **C** may impede the π conjugation, resulting in larger energy gaps than those of the oligomers of series **B**. The band gaps of **A3**–**A7** and **B3**–**B5** are considerably smaller than those of spiro-bridged ladder-type *para*-phenylene oligomers of the same size.[15a]

Conclusion

To the best of our knowledge, prior to this work there have been no examples of the regioselective synthesis of a family of ethene-bridged phenylene oligomers.[14] Herein, we have reported the regiocontrolled syntheses of such oligomers in three distinct classes by using Pt^{II}- and Ru^{II}-catalyzed aromatization. The UV/Vis and PL spectra and the band gaps of these regularly growing arrays showed a pattern of extensive π conjugation with increasing array size. Variable-temperature NMR spectra provided evidence that large arrays of these oligomers are prone to twist from planarity, which hampers their π conjugation. Future use of these ethene-bridged *para*-phenylene oligomers in optoelectronic or nanomaterial devices is under current investigation.

Experimental Section

Solvents and reagents: All experimental operations were performed under nitrogen and the equipment was dried in an oven at 150 °C for several hours. THF was distilled over sodium. DCM and toluene were distilled and dried over calcium hydride. All of the other specified chemicals were commercially purchased (Aldrich and Strem) and used without further purification.

NMR spectroscopic and mass-spectrometric analysis: The ^1H and ^{13}C NMR spectra were determined on a Bruker AV 400 NMR spectrometer and Bruker AVANCE 600 NMR spectrometer in a solution of $CDCl_3$ or $C_2D_2Cl_4$, unless indicated otherwise. Chemical shifts are reported in ppm downfield of the solvent peak ($CDCl_3$: $\delta = 7.24$ ppm for ^1H NMR, $\delta = 77.00$ ppm for ^{13}C NMR) as an internal standard. HRMS was performed on a Finnigan Mat95 mass spectrometer. MALDI mass spectrometry was performed on an AutoflexIII MALDI-TOF mass spectrometer at the National Chung-San University.

Measurement of activation energy: The ^1H variable-temperature NMR spectra of species **A5'** is shown in Figure 2. On increasing the temperature from 25 to 105 °C, the diastereotopic protons of the two singlets (7.772 and 7.739 ppm at 25 °C) of species **C5** coalesced at 105 °C (T_c). The activation energy ($\Delta G^{\neq}$) was calculated by using the equations $K_c = 2.22\Delta\nu$ and $\Delta G^{\neq} = 4.58 T_c(10.32 + \log T_c/K_c)$ cal mol^{-1} (in which $T_c = 378$ K and $\Delta\nu = 16.6$ Hz), which gave a large value of $\Delta G^{\neq} = 19.6 \pm 0.2$ kcal mol^{-1}.

Time-resolved fluorescence measurements: Picosecond time-resolved experiments were performed with a time-correlated single-photon-counting system (TCSPC; PicoQuant Fluotime 200). The excitation pulses at 375 nm were generated from a picosecond laser system (PicoQuant LDH-P-C-375) controlled by a diode laser driver (PicoQuant PDL-800B). The excitation laser was focused onto a cuvette (thickness = 1 cm) containing a sample solution. The fluorescence emitted at a right angle was collected with a lens pair. The wavelength of fluorescence was selected by using a double monochromator (8 nm per mm dispersion, of the subtractive type to correct for distortion of the group velocity dispersion). A multi-channel plate photomultiplier (R3809U-50, Hamamatsu) served as a photon-counting detector from which the signal was fed into a computer with a TCSPC-module (SPC-630, Becker and Hickl) for data acquisition. We selected the polarization of the emission with respect to the excitation laser pulse by using a polarizer. In all experiments reported here, the polarization was fixed at the magic-angle condition (54.7°). The full width at half maximum (FWHM) of the instrument response function (IRF) was determined to be approximately 80 ps.

Steady-state absorption, fluorescence, and quantum yield: The UV/Vis absorption and fluorescence spectra were routinely recorded by using Cary 50 (Varian) and FluoroLog Tau-3 (Jobin Yvon) spectrometers, respectively. The fluorescence quantum yields (Φ_F) of all of the samples in dichloromethane were determined by using a comparative method described in [Eq. (1)], in which the subscripts S and R refer to the sample and reference solutions, respectively.[15–16]

$$\frac{\Phi_F}{\Phi_R} = \frac{n_S^2}{n_R^2} \times \left(\frac{\mathrm{Grad_S}}{\mathrm{Grad_R}}\right) \quad (1)$$

The refractive indexes (n_S and n_R) were used to correct the collection efficiencies of the emissions of different solvents. Grad represents the gradient of the plot of the integrated fluorescence intensity versus absorbance. Anthracene and DPA (9,10-diphenylanthracene) were chosen as the fluorescence standard and its absolute quantum yield was known to be 0.27(±0.03)% in ethanol and 0.90(±0.02)% in cyclohexane at room temperature.[17] Note that the fluorescence spectra of the sample and the reference standard must be recorded at identical experimental conditions so that the relationship shown in [Eq. (1)] holds true. The results obtained according to [Eq. (1)] are summarized in Table 1.

Cyclic voltammetry measurements: The HOMO energy levels of the studied compounds were calculated from the oxidation potential ($E^{1/2}$) obtained from the cyclic voltammetry (CV) measurement with Pt wire as the counter electrode and a glassy carbon electrode as the working electrode. The potentials were measured against an Ag/Ag^+ (0.01 M $AgNO_3$) reference electrode. The final results were calibrated with the ferrocene/ferrocenium (Fc/Fc^+) couple. Under the assumption that the energy level of ferrocene/ferrocenium is 4.8 eV below vacuum, the HOMO energy levels were determined from the equation 4.8 eV + $E^{1/2}$ (versus Fc/Fc^+).

Experimental procedures for the synthesis of A3 (Scheme 6)

Synthesis of compound s1: A mixture of 1,4-dibromo-2,5-diiodobenzene (4.5 g, 9.2 mmol) in DME (1,2-dimethoxyethane, 50 mL) and aqueous K_2CO_3 (46 mL, 20%) was stirred under nitrogen for 10 min. Tetrakis(triphenylphosphine)palladium(0) (531 mg, 0.46 mmol) was added followed by a solution of 4-(2-ethylhexyloxy)phenylboronic acid (5.0 g, 20.2 mmol) in DME (10 mL). The resulting mixture was heated under reflux for 12 h and allowed to cool to room temperature. The organic phase was separated and the aqueous phase was washed with diethyl ether (2 × 100 mL). The combined organic layers were washed with water, brine, and dried with anhydrous $MgSO_4$. The solvent was removed in vacuo and the crude product was purified by a silica column with hexanes, affording compound **s1** (3.86 g, 65%) as a colorless oil.

Synthesis of compound s2: Nitrogen was bubbled through a solution of piperidine (10 mL) and triethylamine (30 mL) for 30 min. Compound **s1** (3.8 g, 5.9 mmol), CuI (112 mg, 0.59 mmol), PPh_3 (155 mg, 0.59 mmol), $Pd(PPh_3)_4$ (341 mg, 0.29 mmol), and ethynyltrimethylsilane (1.85 mL, 13 mmol) were added to this solution. The resulting solution was stirred at 80 °C for 8 h. After cooling to ambient temperature, the solvent was removed in vacuo and the organic layer was extracted with CH_2Cl_2. After concentration in vacuo, the crude material was purified by flash column chromatography on silica gel with ethyl acetate/hexanes (5/95) as the eluent to afford compound **s2** (3.65 g, 91%) as a yellow oil.

Synthesis of compound A3s: *n*-Tetrabutylammonium fluoride (1.0 M) in THF (1.64 mL, 1.64 mmol) was added to a solution of compound **s2** (1.70 g, 1.49 mmol) in THF (20 mL) at 0 °C, and the resulting solution was stirred at 0 °C for 2 h. Column chromatography of the crude material on silica gel with ethyl acetate/hexanes (5/95) as the eluent afforded compound **A3s** (1.46 g, 98%) as a yellow oil.

Synthesis of compound A3: A dry reaction tube containing $[Ru(CH_3CN)_2(PPh_3)Tp][SbF_6]$ (50.2 mg, 0.04 mmol) was dried in vacuo for 2 h before it was charged with compound **A3s** (279 mg, 0.28 mmol) and 1,2-dichloroethane (28 mL). The mixture was heated at 80 °C for 24 h.

 © 2010 Wiley-VCH Verlag GmbH & Co. KGaA, Weinheim

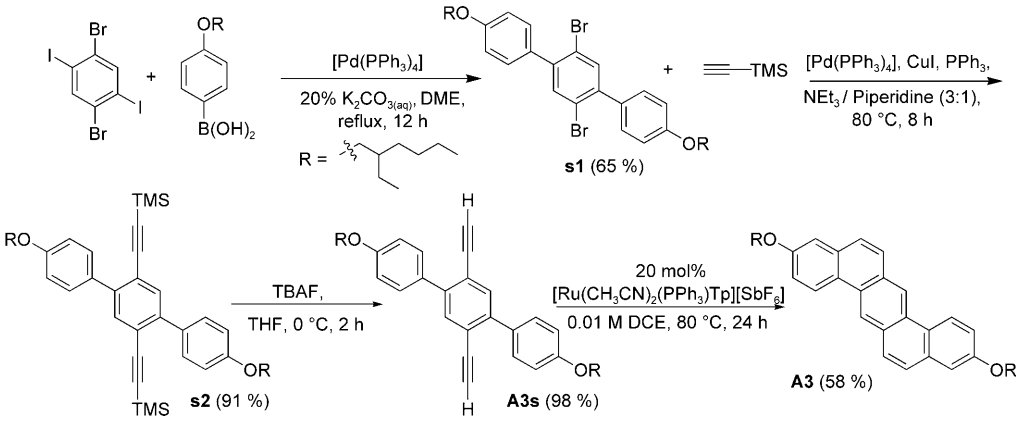

Scheme 6.

After concentration in vacuo, the crude material was purified by flash column chromatography on silica gel by using dichloromethane/hexanes (1/10) as the eluent to afford compound **A3** (162 mg, 58 %) as a white solid.

Spectral data for compound A3s: ^{1}H NMR (400 MHz, $CDCl_3$): $\delta = 7.60$ (s, 2H), 7.56 (d, $J = 8.8$ Hz, 4H), 6.97 (d, $J = 8.8$ Hz, 4H), 3.89 (d, $J = 6.0$ Hz, 4H), 3.14 (s, 2H), 1.79–1.73 (m, 2H), 1.57–1.40 (m, 8H), 1.38–1.32 (m, 8H), 0.97–0.91 ppm (m, 12H); ^{13}C NMR (100 MHz, $CDCl_3$): $\delta =$ 159.2, 142.1, 134.8, 131.0, 130.2, 120.8, 114.0 (2×CH), 82.9, 81.5, 70.4, 39.4, 30.5, 29.1, 23.9, 23.0, 14.1, 11.1 ppm; HRMS calcd for $C_{38}H_{46}O_2$:534.3498; found: 534.3491.

Spectral data for compound A3: ^{1}H NMR (400 MHz, $CDCl_3$): $\delta = 8.97$ (s, 2H), 8.71 (d, $J = 8.8$ Hz, 2H), 7.89 (d, $J = 9.2$ Hz, 2H), 7.64 (d, $J = 8.8$ Hz, 2H), 7.31 (d, $J = 8.8$ Hz, 2H), 7.28 (s, 2H) 4.02 (d, $J = 0.8$ Hz, 4H), 1.83–1.80 (m, 2H), 1.60–1.44 (m, 8H), 1.41–1.35 (m, 8H), 0.98 (t, $J = 7.2$ Hz, 6H), 0.93 ppm (t, $J = 7.2$ Hz, 6H); ^{13}C NMR (100 MHz, $CDCl_3$): $\delta =$ 158.3, 133.3, 130.2, 128.5, 128.0, 126.8, 124.2, 124.2, 121.3, 117.0, 110.1, 70.7, 39.5, 30.6, 29.1, 23.9, 23.1, 14.1, 11.2 ppm; HRMS calcd for $C_{38}H_{46}O_2$:534.3498; found: 534.3491.

Acknowledgements

The authors wish to thank the National Science Council, Taiwan for supporting this work.

[1] a) J. Wu, W. Pisula, K. Müllen, *Chem. Rev.* **2007**, *107*, 718; b) S. Sergeyev, W. Pisula, Y. H. Geerts, *Chem. Soc. Rev.* **2007**, *36*, 1902; c) S. Laschat, A. Baro, Nelli. Steinke, F. Giesselmann, C. Hägele, G. Scalia, R. Judele, E. Kapatsina, S. Sauer, A. Schreivogel, M. Tosoni, *Angew. Chem.* **2007**, *119*, 4916; *Angew. Chem. Int. Ed.* **2007**, *46*, 4832.

[2] For selected examples for discotic BPAHs, see a) H. Sakurai, T. Daiko, T. Hirao, *Science* **2003**, *301*, 1878; b) W. Pisula, A. Menon, M. Stepputat, I. Lieberwirth, U. Kolb, A. Tracz, H. Sirringhaus, T. Pakula, K. Müllen, *Adv. Mater.* **2005**, *17*, 684; c) X. Feng, J. Wu, M. Ai, W. Pisula, L. Zhi, J. P. Rabe, K. Müllen, *Angew. Chem.* **2007**, *119*, 3093; *Angew. Chem. Int. Ed.* **2007**, *46*, 3033; d) M. M. Elmahdy, X. Dou, M. Mondeshki, G. Floudas, H.-J. Butt, H. W. Spiess, K. Müllen, *J. Am. Chem. Soc.* **2008**, *130*, 5311; e) Y.-T. Wu, D. Bandera, R. Maag, A. Linden, K. K. Baldridge, J. S. Siegel, *J. Am. Chem. Soc.* **2008**, *130*, 10729; f) D. C. Harrowven, I. L. Guy, L. Nanson, *Angew. Chem.* **2006**, *118*, 2300; *Angew. Chem. Int. Ed.* **2006**, *45*, 2242; g) T. Nagano, Y. Kiyobayashi, M. Sakiyama, K. Yamamoto, P. C. Cheng, L. T. Scott, *J. Am. Chem. Soc.* **1995**, *117*, 3270.

[3] a) M. Wudl, F. Bendikov, D. F. Perepichka, *Chem. Rev.* **2004**, *104*, 4891; b) J. E. Anthony, *Chem. Rev.* **2006**, *106*, 5028; c) M. J. Panzer, C. D. Frisbie, *J. Am. Chem. Soc.* **2005**, *127*, 6960; d) M. M. Payne, S. R. Parkin, J. E. Anthony, *J. Am. Chem. Soc.* **2005**, *127*, 8028; e) H. Meier, *Angew. Chem.* **2005**, *117*, 2536; *Angew. Chem. Int. Ed.* **2005**, *44*, 2482; f) R. Mondal, C. Tonschoff, D. Khon, D. C. Neckers, H. F. Bettinger, *J. Am. Chem. Soc.* **2009**, *131*, 14281.

[4] a) D. Chun, Y. Cheng, F. Wudl, *Angew. Chem.* **2008**, *120*, 8508; *Angew. Chem. Int. Ed.* **2008**, *47*, 8380; b) I. Kaur, N. N. Stein, R. P. Kopreski, G. P. Miller, *J. Am. Chem. Soc.* **2009**, *131*, 3424; c) J. Briggs, G. P. Miller, *Org. Lett.* **2003**, *5*, 4203.

[5] For selected examples of important ribbon-typed BPAHs other than polyacenes, see: a) Y. Nakamura, N. Aratani, H. Shinnokubo, A. Takagi, T. Kawai, T. Matsumoto, Z. S. Yoon, D. Y. Kim, T. K. Ahn, D. Kim, A. Muranaka, N. Kobayashi, A. Osuka, *J. Am. Chem. Soc.* **2006**, *128*, 4119; b) X. Qiao, M. A. Padula, D. M. Ho, N. J. Vogelaar, C. E. Schutt, R. A. Pascal, Jr., *J. Am. Chem. Soc.* **1996**, *118*, 741; c) N. G. Pschirer, C. Kohl, F. Noble, J. Qu, K. Müllen, *Angew. Chem.* **2006**, *118*, 1429; *Angew. Chem. Int. Ed.* **2006**, *45*, 1401.

[6] a) M. B. Goldfinger, T. M. Swager, *J. Am. Chem. Soc.* **1994**, *116*, 7895; b) J. D. Tovar, T. M. Swager, *J. Org. Chem.* **1999**, *64*, 6499; c) M. C. Bonifacio, C. R. Robertson, J.-Y. Jung, B. T. King, *J. Org. Chem.* **2005**, *70*, 8522; d) H.-C. Shen, J.-M. Tang, H.-K. Chang, C.-W. Yang, R.-S. Liu, *J. Org. Chem.* **2005**, *70*, 10113; e) F. B. Mallory, K. E. Butler, A. Berube, E. D. Luzik, Jr., C. W. Mallory, E. J. Brondyke, R. Hiremath, P. Ngo, P. J. Caroll, *Tetrahedron* **2001**, *57*, 3715.

[7] H. Okamoto, N. Kawasaki, Y. Kaji, Y. Kubozono, A. Fujiwara, M. Yamaji, *J. Am. Chem. Soc.* **2008**, *130*, 10470.

[8] a) V. Mamane, P. Hannen, A. Fürstner, *Chem. Eur. J.* **2004**, *10*, 4556; b) A. Fürstner, V. Mamane, *J. Org. Chem.* **2002**, *67*, 6264.

[9] R. O. C. Norman, J. M. Coxon in *Principles of Organic Synthesis*, 3rd ed., Blackie Academic & Professional, Glasgow, **1993**, p. 68.

[10] Similar behaviors were observed for pyrazine-containing polyacenes, see: B. Gao, M. Wang, Y. Cheng, L. Wang, X. Jing, F. Wang, *J. Am. Chem. Soc.* **2008**, *130*, 8297.

[11] Ruthenium-catalyzed aromatization was shown to involve ruthenium-vinylidene intermediates (I).[11] In the ruthenium catalysis, we did not obtain different regioisomers because the corresponding in-

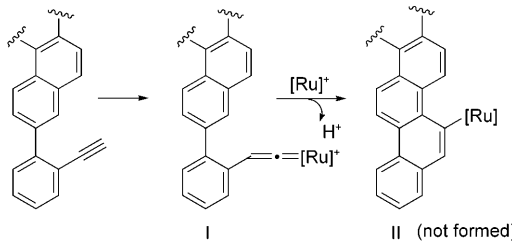

 © 2010 Wiley-VCH Verlag GmbH & Co. KGaA, Weinheim

termediate (II) suffers great steric hindrance between aromatic array and bulky ruthenium fragment..

[12] For selected examples of the aromatization of dienynes with [Ru-$(CH_3CN)_2(PPh_3)Tp][SbF_6]$ and other ruthenium catalysts, see: a) S. Datta, A. Odedra, R.-S. Liu, *J. Am. Chem. Soc.* **2005**, *127*, 11606; b) H.-C. Shen, S. Pal, J.-J. Lian, R.-S. Liu, *J. Am. Chem. Soc.* **2003**, *125*, 15762; c) P. M. Donovan, L. T. Scott, *J. Am. Chem. Soc.* **2004**, *126*, 3108.

[13] For the planarity twist of a discotic BPAH, see: a) R. A. Pascal, Jr., *Chem. Rev.* **2006**, *106*, 4809; b) Y. Wang, A. D. Stretton, M. C. McConnel, P. A. Wood, S. Parsons, J. B. Henry, A. R. Mount, T. Galow, *J. Am. Chem. Soc.* **2007**, *129*, 13193; c) T. Baird, J. H. Gall, D. D. MacNicol, P. R. Malliinson, C. R. Michie, *Chem. Commun.* **1988**, 1471; d) G. A. Downing, C. S. Frampton, D. D. MacNicol, P. R. Malliinson, *Angew. Chem.* **1994**, *106*, 1653; *Angew. Chem. Int. Ed. Engl.* **1994**, *33*, 1587.

[14] a) J. Grimme, M. Kreyenschmidt, F. Uckert, K. Müllen, U. Scherf, *Adv. Mater.* **1995**, *7*, 292; b) A. Kraft, A. C. Grimsdale, A. B. Holmes, *Angew. Chem.* **1998**, *110*, 416; *Angew. Chem. Int. Ed.* **1998**, *37*, 402.

[15] For selected examples of ladder-type *para*-phenylene oligomers, see: a) Y. Wu, J. Zhang, Z. Bo, *Org. Lett.* **2007**, *9*, 4435; b) F. Schindler, J. Jacob, A. C. Grimsdale, U. Scherf, K. Müllen, J. M. Lupton, J. Feldmann, *Angew. Chem.* **2005**, *117*, 1544; *Angew. Chem. Int. Ed.* **2005**, *44*, 1520.

[16] C.-W. Chang, C. K. Chou, I-J. Chang, Y.-P. Lee, E. W.-G. Diau, *J. Phys. Chem. A* **2007**, *111*, 13288.

[17] B. Valeur, *Molecular Fluorescence: Principles and Applications*, Wiley-VCH, Weinheim, **2001**.

[18] A. T. R. Williams, S. A. Winfield, J. N. Miller, *Analyst* **1983**, *108*, 1067.

Received: August 11, 2009
Published online: December 22, 2009

 © 2010 Wiley-VCH Verlag GmbH & Co. KGaA, Weinheim